(Preprint) AAS 24-126

ROBUST OPTIMIZATION WITH AUTONOMOUS OPTICAL-ONLY SPACECRAFT-TO-SPACECRAFT NAVIGATION IN CISLUNAR SPACE

Sergio Bonaccorsi*, Pierluigi Di Lizia†

Autonomous navigation for spacecraft missions in cislunar space would greatly reduce the workload of ground stations, which is going to significantly increase in the next years. This study evaluates the performance of a spacecraft-to-spacecraft optical-only navigation strategy and perform a robust trajectory optimization according to a recently introduced mission analysis approach. This merges classical nominal trajectory design with a complete navigation assessment within the same optimization process. The results show that this autonomous navigation strategy may become a valid alternative for limited-capability spacecraft relying on low-cost sensors in cislunar space. The flexibility of such method evokes great curiosity and interest, given the larger degrees of freedom available during the mission design phase.

INTRODUCTION

The growing interest in lunar missions is expected to lead to a significant increase in the number of spacecraft operating in lunar and cislunar regimes. At the same time, space exploration is increasingly leveraging small platforms like SmallSats and CubeSats, which offer cost-effective opportunities for scientific and technological advancements. This scenario of an increasing space object population in the cislunar regime, mainly composed by small spacecraft, poses a dual challenge. On one hand, this expansion will generate a greater burden on ground stations responsible for mission operations, making it impractical to support navigation for all future missions solely through ground-based services. On the other hand, small spacecraft are characterized by limited capabilities related to restricted control authority, large navigation uncertainties, and actuation errors, thus leading to navigation costs of the same order of magnitude of the nominal ones computed through the traditional mission design.[1] In this context, autonomous navigation and robust optimization techniques may represent valid options to mitigate these problems and face the incoming new challenges of space missions.

For missions in cislunar space, involving large distances from Earth, the baseline option for orbit determination is generally ground-based radiometric navigation, often relying on the Deep Space Network (DSN). However, scheduling observations with Earth-based radars like the DSN is becoming increasingly difficult. At the same time, Earth-based optical telescopes face specific limitations, such as needing to avoid exclusion zones near the Moon to protect sensors from excessive light exposure. In general, ground-based observations suffer from restricted viewing geometries for cislunar

*PhD Candidate, Department of Aerospace Science and Technology, Politecnico di Milano, Via La Masa 34, 20156 Milan, Italy.
†Associate Professor, Department of Aerospace Science and Technology, Politecnico di Milano, Via La Masa 34, 20156 Milan, Italy.

objects, leading to sparse data collection and extended periods of occultation.[2] On the contrary, a space-based measurement acquisition process can rely on reduced sensor-to-target distances, longer data arcs and higher Signal-to-Noise Ratio (SNR), thus playing a pivotal role in this context. Space-based autonomous navigation strategies currently focus on several approaches. One of the most studied is vision-based navigation using images of various targets, such as lunar landmarks or lunar limb.[3] Another relevant approach relies on spacecraft-to-spacecraft measurements, such as the LiAISON method, which uses range-only measurements to allow co-estimation of the inertial states of both satellites leveraging unique trajectories from three-body dynamics.[4] In this context, Greaves and Scheers found that optical-only measurements achieve faster state observability than range-only ones.[5] This approach is particularly relevant given the low-cost sensors commonly employed in the design of small spacecraft. However, careful consideration must be given to ensuring the success of the measurement acquisition process, especially under stringent visibility constraints. This means that both the mission analysis process and the optical payload design must take into account different challenges of this scenario.

The high navigation costs for small spacecraft missions are strongly dependent on the uncertainties arising from the navigation process and the command execution errors. Robust optimization techniques, extensively studied in recent years, address this challenge by enhancing mission reliability and feasibility under uncertainty. In this field, a mission analysis approach, firstly introduced by Giordano and Topputo, aims to integrate orbit determination and trajectory correction maneuvers into trajectory design, in order to optimize both deterministic and stochastic costs.[1] In their work, the authors formulate an alternative statement to the classical sequential approach by introducing the so-called *Integrated approach*. Their goal is to merge, since the preliminary design phase, the nominal trajectory optimization with a complete navigation assessment.

This study aims to evaluate the potential of space-based autonomous navigation and robust optimization methods in addressing the challenges of cislunar navigation for limited-capability spacecraft. Specifically, it first examines the capabilities and limitations of an autonomous navigation method based on spacecraft-to-spacecraft optical-only measurements. The study then seeks to enhance the performance of this navigation strategy by applying a robust trajectory optimization process. The objectives are to assess the effectiveness of this novel space-based navigation technique compared to traditional ground-based systems and to explore its role in improving trajectory design robustness. To investigate these concepts, the study focuses on the orbital transfer phase from an injection selenocentric orbit to the operational Halo orbit of the LUMIO satellite.[6] Trajectory design follows the integrated approach, incorporating both deterministic and stochastic costs. Navigation operations are simulated using both ground-based and space-based methods to compare their performance. Optical measurements are modeled with specific constraints to ensure realism. The results and insights are drawn from a diverse set of solutions to capture potential variations. The subsequent sections detail these aspects, including methodology, analysis, and main results.

The approaches for robust mission design are presented, starting with the classical sequential approach and moving on to the Integrated approach and a revised version introduced by this work. The building blocks of the formulation are then explained, providing the most relevant information regarding the uncertainty propagation method, the navigation algorithms, and the guidance law used to compute the TCMs. Next, the test case scenario is described, including the timeline of operations, beacon orbit selection, and the complete procedure for obtaining numerical results. Key observations on the results are subsequently discussed. Finally, the conclusions summarize the main findings, highlight the objectives achieved, and propose directions for future research.

PROBLEM STATEMENT

As stated in the introduction, extensively studies have been carried out in the recent years in the field of optimization methods for robust mission design. For the purposes of this work, only the approaches used to get the numerical results will be recalled. In particular, the traditional sequential approach is firstly described, followed by the Integrated approach and its revised version, the Multi-step approach. To provide better context for these mission design frameworks, the test case of the LUMIO orbital transfer is first introduced, serving as a reference for the algorithms explained in the subsequent sections. The motion of the satellite is considered to be modeled by the dynamics of the Circular Restricted Three Body Problem (CR3BP).[7]

LUMIO Orbital Transfer

The test case scenario presented in Reference 1, and proposed also for this study, is the orbital transfer phase from an injection selenocentric orbit to the operative halo orbit of the LUMIO satellite.[6] In this phase, an impulsive maneuver, which is called Stable Manifold Injection Maneuver (SMIM), places the spacecraft onto the stable manifold of the target halo. Then, a Halo Injection Maneuver (HIM) finally injects the satellite into the target orbit. Considering this scenario, a nominal mission timeline is selected (Figure 1), which includes two Orbit Determination (OD) windows that are used to correctly estimate the two subsequent Trajectory Correction Maneuvers (TCMs). This mission timeline was selected based on preliminary analyses indicating the potential for relative visibility between LUMIO and the chosen ground station, thereby ensuring an effective navigation process. One has to consider the cut-off time elapsing between the computation of the state estimate at the end of the OD operations, and the sending of the command of the TCM from the ground. This also implies that the satellite must be again in relative visibility to allow for the reception of the incoming signal. In the case of an autonomous guidance operation, the satellite may be considered able to perform the correction maneuver without exchanging signals with the ground.

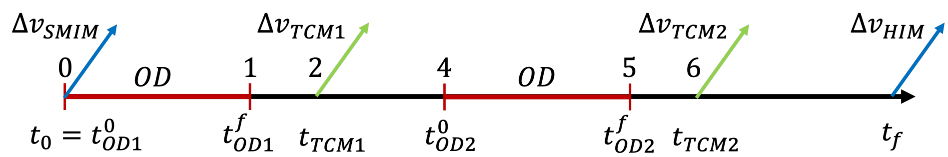

Figure 1. Timeline of the orbital transfer phase. The red bars represent the OD phases, while the green arrows mark the TCMs points, and the blue arrows mark the two deterministic impulses. Times, indicated above the timeline, are in days after the SMIM.

Sequential Approach

The traditional approach to robust mission design involves computing a nominal trajectory, evaluating its statistical properties, and determining the navigation costs. This process, extensively detailed in the literature, is divided into two sequential and independent steps.[8] The first is the design of the nominal trajectory within a deterministic optimization framework, typically aimed at minimizing fuel consumption while satisfying physical constraints, such as position continuity between transfer legs.

The second step is the *navigation assessment*, which comprises the knowledge analysis and navigation cost estimation. The first involves performing a covariance analysis to estimate the accuracy of the spacecraft state knowledge, specifically the deviation of the estimated state from the true one. During this phase, the state covariance is propagated over time using uncertainty propagation methods, which predict an expected growth in uncertainty. Orbit determination phases, during which measurements are acquired and processed through state estimation algorithms, are then used to reconstruct the spacecraft state and reduce its associated covariance. Consequently, knowledge covariance increases during propagation but decreases during OD phases.

Finally, a stochastic analysis is conducted to estimate the navigation costs required to ensure the spacecraft reaches its target. This step relies on a guidance law to compute the TCMs, which will be detailed later. At the conclusion of this process, the trajectory dispersion, representing the deviation of the true spacecraft state from the nominal trajectory, can be evaluated.

Integrated Approach

This section outlines the innovative approach to robust mission design introduced by Giordano and Topputo in Reference 1, which is recommended for further reading for more detailed explanations.

The main goal of the Integrated approach is to minimize both the deterministic and stochastic costs within a single optimization framework. In other words, the free variables associated to the nominal trajectory design and the navigation assessment are optimized at the same time with a minimum fuel objective. An innovation of this approach is to include the stochastic aspects related to both the physical constraints and the cost function in the optimization routine. For the first, the continuity in position is converted into a bounded final dispersion of the samples. For the second, the costs associated to the TCMs are included by relying on their statistical representation through the 99-percentile.

The trajectory design process begins with the computation of an educated initial guess within a deterministic framework. This step minimizes the deterministic costs associated with the two impulses while enforcing position continuity through a final constraint. The Integrated approach is then applied, starting with the initial nominal state, its associated dispersion, and initial knowledge, which are propagated forward in time. At specific intervals, an OD process is conducted to estimate the true trajectory and reduce the knowledge covariance. The estimated trajectory is then used to inform a guidance scheme, compute correction maneuvers, and minimize dispersion. Ultimately, the final nominal state and its dispersion are obtained. These steps allow for the computation of both the deterministic and stochastic costs, which are used to define the cost function to be minimized, together with the final dispersion, which is used to satisfy the stochastic constraint at the final time.

Multi-step Approach

This work considers a slightly revised version of the original formulation of the Integrated approach. A multi-step optimization sequence has been adopted, instead of a single optimization algorithm. Each step considers a reduced number of free variables and some new ones with respect to the original framework. This choice has been pursued in order to isolate specific variables and therefore assess their role in influencing the minimization of the cost function and the satisfaction of the stochastic final constraint, which consists in a bounded dispersion around the target point.

The first step of this optimization sequence is called *Preliminary Integrated Approach* (P-IA), in which the free variables are only the epochs of the TCM execution, while the rest remain fixed. Then, the *Navigation-focused Integrated Approach* (N-IA) considers only the initial epoch of the navigation window and the epoch of the subsequent TCM among the free variables. Finally, the original version of the algorithm, here denoted as *Full Integrated Approach* (F-IA) is applied. Along this resolution procedure, the final constraint is also modified step by step, increasing the level of requested accuracy. In addition, the initial guess of each step of the algorithm is the solution of the previous step. Along this document, all these steps will be compared to the typical *Sequential Approach* (SA).

In the following, the formulation of the optimization problem to be solved for each step is reported. The vector of free variables will be referred to as $\mathbf{y}$, the scalar cost function as J, the inequality constraint as c, while the notation $\hat{F}_d(\cdot)$ refers to the estimated value of the Cumulative Distribution Function (CDF) evaluated at the specific value, and $Q(\cdot,\cdot)$ refers to the quantile evaluated at the threshold given by the first input for the quantity given by the second input. The N-IA includes two steps, one for each OD phase shown in Figure 1.

For what concerns the free variables, τ_0 is the initial epoch, τ_f is the final epoch, τ_{TCM_1} and τ_{TCM_2} refer to the epochs of TCMs execution, $\tau^0_{\text{OD}_1}$ and $\tau^0_{\text{OD}_2}$ refer to the initial epochs of the OD windows, $\boldsymbol{\alpha}_0$ refers to the vector containing the orbital parameters of the injection selenocentric orbit, and $\boldsymbol{\Delta}\mathbf{v}_{\text{SMIM}}$ refers to the first deterministic impulsive maneuver vector.

Preliminary Integrated Approach. Find $\mathbf{y} = [\tau_{\text{TCM}_1}, \tau_{\text{TCM}_2}]$, such that

$$J = Q(.99, \Delta v_{\text{TCM}_1}) + Q(.99, \Delta v_{\text{TCM}_2})$$

is minimized, with the state subjected to initial constraints on position, velocity, knowledge covariance and distribution. As a final constraint, a measure of the distance of the real trajectories from the target halo is introduced, by exploiting the Kernel Quantile Estimation method. This will force the solution to have the 90% of the samples within a sphere of 60 km radius.

$$c = \hat{F}_d(60\ \text{km}) > 0.90$$

Navigation-focused Integrated Approach.

- **Step 1:** Find $\mathbf{y} = [\tau^0_{\text{OD}_1}, \tau_{\text{TCM}_1}]$, such that

  $$J = Q(.99, \Delta v_{\text{TCM}_1}) + Q(.99, \Delta v_{\text{TCM}_2})$$

  is minimized. As a final constraint:

  $$c = \hat{F}_d(50\ \text{km}) > 0.90$$

- **Step 2:** Find $\mathbf{y} = [\tau^0_{\text{OD}_2}, \tau_{\text{TCM}_2}]$, such that

  $$J = Q(.99, \Delta v_{\text{TCM}_1}) + Q(.99, \Delta v_{\text{TCM}_2})$$

  is minimized. As a final constraint:

  $$c = \hat{F}_d(40\ \text{km}) > 0.95$$

Full Integrated Approach.[1] Find $\mathbf{y} = [\tau_0, \tau_f, \tau_{\text{TCM}_1}, \tau_{\text{TCM}_2}, \boldsymbol{\alpha}_0, \boldsymbol{\Delta}\mathbf{v}_{\text{SMIM}}]$, such that

$$J = \Delta v_{\text{SMIM}} + \Delta v_{\text{HIM}} + Q(.99, \Delta v_{\text{TCM}_1}) + Q(.99, \Delta v_{\text{TCM}_2})$$

is minimized. As a final constraint:

$$c = \hat{F}_d(30\text{ km}) > 0.95$$

For the purposes of this work, while Reference 1 considers only a ground-based navigation method to perform the orbit determination operations, here both a ground-based and the previously mentioned space-based strategies are used in order to compare their performance on the same mission scenario.

Some preliminary considerations must be highlighted regarding this formulation of the optimization process. As outlined for the original version of the Integrated approach, also in this case the trajectory design begins with the computation of an initial guess within a deterministic framework. This is then used as input for the first step of the optimization sequence. It must be remarked that this is already a feasible solution for the orbital transfer, as it satisfies all relevant physical constraints. However, given that its robustness has not yet been assessed, it is considered only as a first guess for the robust optimization process.

Then, another relevant point is that only the F-IA acts on the variables that influence the nominal trajectory, specifically the set of orbital parameters $\boldsymbol{\alpha}_0$ and the first impulsive maneuver vector $\boldsymbol{\Delta}\mathbf{v}_{\text{SMIM}}$. This means that the first steps of the approach focus on optimizing the variables affecting the navigation costs and the dispersion around the final target, thereby enhancing robustness against uncertainties. Subsequently, the F-IA step of the algorithm optimizes the variables of the nominal solution, identifying a trajectory whose deterministic characteristics also ensure improved robustness and overall performance.

METHODOLOGY

Several building blocks can be identified for the earlier presented approach. During the ballistic phase of the transfer, when no measurements are available and no state estimation algorithms are applied, the state and its associated covariance must be propagated in time. This requires an appropriate uncertainty propagation method capable of accurately quantifying stochastic quantities and managing the significant covariance growth expected under the highly nonlinear dynamics of the cislunar regime.

When navigation operations are performed, measurements are first simulated according to the selected model. For the ground-based strategy, these measurements consist of range data acquired from an Earth-based DSN radar. For the space-based navigation strategy, angles-only measurements are simulated, assuming that LUMIO points at a target spacecraft in an Near-Rectilinear Halo Orbit (NRHO). The OD process is then simulated by processing these measurements within an Extended Kalman Filter (EKF). The EKF has proven to be both accurate for this scenario and suitable for a potential onboard implementation of space-based navigation operations.

Once the spacecraft state is estimated through the OD process, it is fed into a guidance law to compute the required TCMs. As a consequence, the stochastic costs strongly depend on the accuracy of the estimate obtained from the navigation operations. The following subsections provide a description of the models used to implement these fundamental building blocks of the robust mission design approach.

Uncertainty Propagation

The test case selected for this work presents peculiar aspects that can be considered in order to make a reasonable and suitable choice for the uncertainty propagation and quantification method. First, due to the chaotic nature of cislunar dynamics, the method must effectively handle nonlinearities. Second, the propagation time is relatively short, as the duration of the transfer phase should be on the order of days. Finally, and most critically, the method must be computationally efficient to integrate within an optimization algorithm, enabling cost-effective quantification of stochastic quantities in a Monte Carlo-like framework.

For these reasons, a hybrid method based on the Polynomial Chaos Expansion (PCE) and the Conjugate Unscented Transform (CUT) is selected. The first is a nonlinear uncertainty quantification technique, in which the input uncertainties and the solution are approximated using a series expansion based on some orthogonal polynomials. The second is an extension of the Unscented Transform (UT), as it generates the sigma points on some peculiar non-principal axes of the initial distribution function, thus enabling the possibility to correctly estimate higher order moments of stochastic integrals.[9]

The core idea behind this method, called PCE-CUT, is that the numerical integration for computing the generalized Fourier PCE coefficients of the series expansion can leverage the quadrature nodes selected according to the sigma points generated by the CUT. This means that, throughout the operations of the optimization algorithm, only the sigma points generated from the initial state and covariance are propagated to the epochs of interest to calculate the PCE coefficients. Then, the PCE is used to inexpensively produce a large number of samples at those specific epochs, thus enabling the computation of stochastic quantities such as the 99-percentile of the TCMs cost and the final dispersion through kernel estimation techniques.

In the following, only the main concepts of the mathematical framework of the PCE-CUT are reported in order to make the method easier to understand. For further information about the contents of this section, the reader is highly encouraged to refer to Reference 1, where a well detailed description and justification of the mathematical formulation for this uncertainty propagation method is reported.

According to the PCE, the approximate estimate of a stochastic variable of interest can be expressed as

$$\hat{\mathbf{x}}(t, \boldsymbol{\xi}) = \sum_{\alpha \in \Lambda_{p,d}} \mathbf{c}_\alpha(t) \psi_\alpha(\boldsymbol{\xi}) \tag{1}$$

where $\Lambda_{p,d}$ is a set of the multi-index of size d and order p defined on nonnegative integers, $\boldsymbol{\xi} = [\xi_1, \ldots, \xi_d]$ is the set of input random variables, in which each element ξ_i is an independent identically distributed variable. The basis functions $\{\psi_\alpha(\boldsymbol{\xi})\}$ are multidimensional spectral polynomials, orthonormal with respect to the joint probability measure $\rho(\boldsymbol{\xi})$ of the vector $\boldsymbol{\xi}$.

Generation of a PCE means computing the generalized Fourier coefficients $\mathbf{c}_\alpha(t)$ by projection of the exact solution $\mathbf{x}(t, \boldsymbol{\xi})$ onto each basis function $\psi_\alpha(\boldsymbol{\xi})$, truncated at the total order p

$$\mathbf{c}_\alpha(t) = E\left[\mathbf{x}(t,\cdot)\psi_\alpha(\cdot)\right] = \int_{\Gamma^d} \mathbf{x}(t,\boldsymbol{\xi})\psi_\alpha(\boldsymbol{\xi})\rho(\boldsymbol{\xi})\mathrm{d}\xi \tag{2}$$

According to the non-intrusive method based on pseudospectral collocation selected for this work, numerical integration of Equation 2 can be performed by collocating $\mathbf{x}(t,\boldsymbol{\xi})$ on certain quadrature nodes defined on Γ^d in order to find $\mathbf{c}_\alpha(t)$.

$$\mathbf{c}_{\boldsymbol{\alpha}}(t) \simeq \mathcal{Q}\left[\mathbf{x}(t,\cdot)\psi_{\boldsymbol{\alpha}}(\cdot)\right] = \sum_{q=1}^{M} \mathbf{x}\left(t,\xi_q\right)\psi_{\boldsymbol{\alpha}}\left(\xi_q\right)\omega_q \tag{3}$$

where $\boldsymbol{\xi}_q$ is the set of quadrature nodes, ω_q are the quadrature weights, and $\mathcal{Q}$ is the quadrature scheme.

Thus, CUT can be seen as a way to compute the stochastic integral given in Equation 3 through a quadrature scheme. This means that, throughout the operations of the optimization algorithm, only the sigma points generated by the CUT have to be propagated, thus largely reducing the computational burden with respect to other quadrature scheme or a typical Monte Carlo simulation.

This method is crucial for the execution of the algorithm, since it is capable of accurately quantifying the stochastic quantities within the optimization solver without performing an expensive Monte Carlo analysis.

Ground-based Measurement Model

For the ground-based navigation strategy, the use of an Earth-based radar of the DSN in Goldstone has been chosen. The sensor is considered to be able to acquire both range and range rate measurements (ρ and $\dot{\rho}$ respectively), according to some visibility constraints.

The model for the simulation of the measurements therefore implies the computation of both the relative position and velocity vectors, respectively $\mathbf{r}$ and $\dot{\mathbf{r}}$, between the ground station and LUMIO.

$$\rho = \sqrt{\mathbf{r}^T\mathbf{r}} \qquad \dot{\rho} = \frac{1}{\rho}\mathbf{r}^T\dot{\mathbf{r}} \tag{4}$$

Measurements are then simulated only if a link between the spacecraft and the selected ground station can be established. This means that, for each OD phase, a visibility window is identified if the Sun exclusion angle is larger than 0.5 deg and if the spacecraft elevation is above a minimum of 5 deg. A simplified graphical representation of the measurement acquisition process is shown in Figure 2, while in Table 1 the numerical values for the constraints are reported.

Table 1. Values for the constraints to be set for the ground-based navigation strategy.

Constraint	Threshold
Sun exclusion angle δ	0.5 deg
Minimum elevation angle ϕ	5 deg

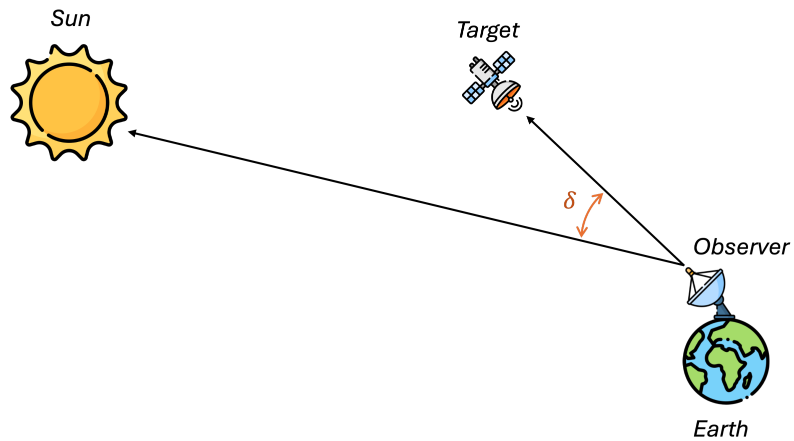

Figure 2. Illustration of the relative geometry between the Observer (an Earth-based radar in this case), the Target (LUMIO), and the Sun. The figure shows the Target angle with respect to the Sun (δ) when pointed by the Observer.

Space-based Measurement Model

For the autonomous space-based navigation strategy, the optical-only spacecraft-to-spacecraft method has been chosen. This approach uses inter-satellite measurements to estimate the inertial states of both spacecraft involved in the navigation process. As highlighted in the introduction, the feasibility of estimating the inertial states of two satellites, rather than just their relative state, was first demonstrated by Hill and Born.[4] Their LiAISON method relies on range-only or combined range and range-rate measurements between satellites, achieving full state observability due to the asymmetric gravity field in the cislunar regime, influenced by the Earth and the Moon.

Many research works extended this concept to angles-only navigation, which is the method selected for this study to evaluate the potential of inter-satellite autonomous navigation. This approach provides two main advantages as it greatly reduces the workload on ground operations and mitigates the visibility constraints by relying on shorter distances between the observer and the target.

The simulation of angles-only measurements begins with the computation of the orbital states of both the observer and the target using the selected dynamical model, which in this case is the CR3BP. This allows to obtain the observer position vector $\mathbf{r}_O$ and the target position vector $\mathbf{r}_T$. These are used to compute the relative position vector $\mathbf{r}$ and the resulting angles-only measurements according to the following model.

$$Az = \tan^{-1}\left(r_y/r_x\right) \qquad El = \sin^{-1}\left(r_z/r\right) \tag{5}$$

Where r_x, r_y, r_z are the components of the relative position vector $\mathbf{r}$, and r is its module.

As stated in the introduction, these angles-only measurements are acquired by a space-based optical sensor, which does not rely on the active illumination of the object and hence is entirely passive. In order to model the measurement process of an optical sensor, the magnitude of a representative space object is computed according to a suitable model.[10] In particular, a cannonball model is used for a spherical object, which provides a reasonable baseline for visibility conditions in a preliminary analysis.[11]

$$V = V_{Sun} - 2.5 \log_{10} \frac{A\varepsilon}{r^2} \frac{2}{3\pi^2} (\sin\alpha + (\pi - \alpha)\cos\alpha) \tag{6}$$

Here V_{Sun} is the apparent reference magnitude of the Sun, equal to -26.78, r is the distance between the target and the observer, A is the object's area, here set to 1 m^2, ε is the bond albedo, here set to 0.3, and α is the phase angle between the Sun and the observer at the target's location, as also shown in Figure 3.

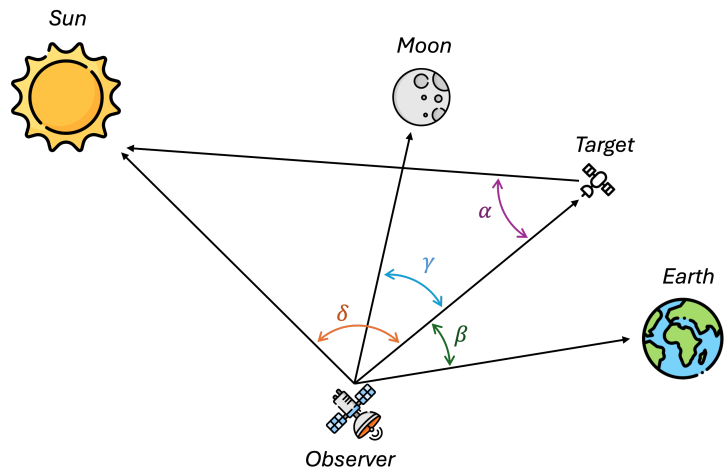

Figure 3. Illustration of the relative geometry between the Observer (LUMIO in this case), the Target, the Sun, the Earth, and the Moon. The figure shows the phase angle viewed from the Target (α), the Target angle with respect to the Sun (δ), the Target angle with respect to the Earth (β), the Target angle with respect to the Moon (γ) when pointed by the Observer.

Orbital propagation within the CR3BP, which is an autonomous model, produces position and velocity data associated with a nondimensional time interval and expressed in a synodic reference frame. Each satellite state is then converted from the synodic frame to the ECI J2000 reference frame using the appropriate rotation model.[12]

To perform this conversion, a specific initial date for the operations is chosen, and the nondimensional propagation time vector is transformed into a dimensional time axis. This step ensures consistency in subsequent operations, as planetary ephemerides, retrieved from SPICE, are provided in the ECI J2000 reference frame at a specific epoch.

Once the state of the observer, the target, the Sun, the Moon, and the Earth in the ECI J2000 reference frame at a specific epoch are available, the quantities required for evaluating all relevant visibility constraints can be computed. In particular, starting from the illustration in Figure 3, the exclusion angles of the Sun δ, the Earth β, and the Moon γ can be determined by using the specific relative position vectors between the target, the observer, and the body of interest. For the target to be visible, considering the thresholds reported in Table 2, these angles must overcome the thresholds, while the visual magnitude must be lower than the limiting value.

Next, the possibility that the target is obscured due to occultation by the Earth or the Moon is considered. As illustrated in Figure 4, the target is deemed visible only if the angle ϕ is larger than the minimum angle ϕ_{min}, which is computed based on the radius of the occulting body. Although

Figure 4 depicts the specific case of the Moon as the occulting body, the same considerations apply to the Earth.

Finally, the possibility that the target is not illuminated by the Sun due to an eclipse caused by the Earth or the Moon is also considered. In this case, the conical model and the considerations reported in Reference 13 are applied. Referring to the illustration in Figure 5, the apparent radii of the Sun and the Moon are computed based on the angles θ_{Sun} and θ_{Moon}. Using the relative position vectors from the Sun to the target and from the Moon to the target, the apparent separation of their centers θ_{app} is calculated through a SPICE routine. If the following condition is satisfied, the object is considered to be within the shadow cone, and therefore not illuminated by the Sun and not visible to the observer.

$$\theta_{\mathrm{app}} < \theta_{\mathrm{Moon}} - \theta_{\mathrm{Sun}} \tag{7}$$

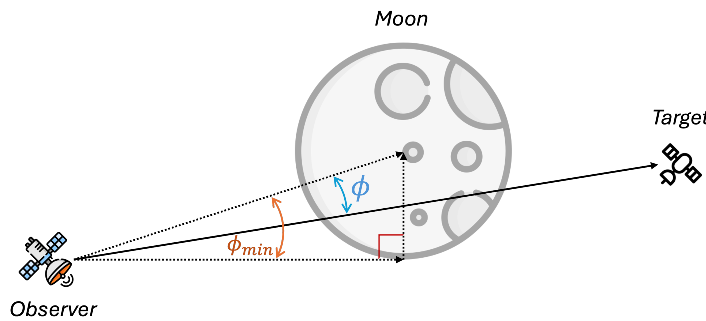

Figure 4. Illustration of the possible obstruction of the Moon between the Observer (LUMIO in this case) and the Target.

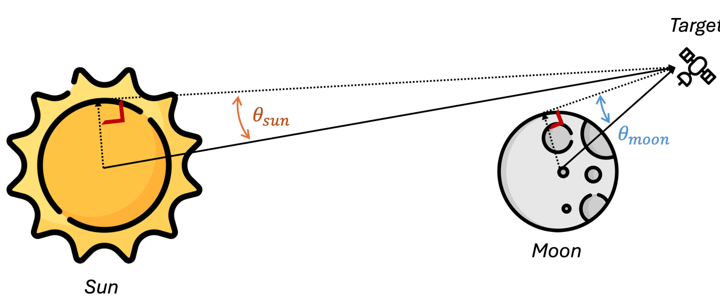

Figure 5. Illustration of the angles for the computation of the apparent radius of both the Sun and the Moon for the eclipse conical model. The same model is used for the Earth.

Table 2. Values for the constraints to be set for the space-based navigation strategy.

Constraint	Threshold
Sun exclusion angle δ	50 deg
Earth exclusion angle β	35 deg
Moon exclusion angle γ	30 deg
Visual magnitude V	16

Guidance Law

The operations to be followed during the navigation assessment, in which the stochastic costs associated to the selected solution are computed, require the definition of a guidance law. This is an algorithm that takes as input the estimated state of the satellite obtained at the end of OD phase, and which gives as output the TCM that is needed to apply to the spacecraft in order to compensate the deviation with respect to the reference trajectory. The goal of correction maneuvers is to reduce the dispersion with small fuel consumption.

For this work, the Differential Guidance (DG) algorithm, a common choice for the computation of TCMs in the case of deep-space missions, is selected.[14] The DG is a linearized approach aiming at compensating the deviation of the current actual state of the spacecraft with respect to the reference one by relying on the use of two impulsive maneuvers within the selected leg. In practice, the second of these impulses is not executed, as a new maneuver can be computed at the final leg time, allowing the entire algorithm to be repeated in a receding horizon approach.

Considering a relatively short time duration between the execution of the TCMs, the DG relies on a first-order approximation, allowing for the computation of the impulsive maneuver according to the following model.[15]

$$\Delta \mathbf{v}_j^s = -\left(\Phi_{rv}^T \Phi_{rv} + q \Phi_{vv}^T \Phi_{vv}\right)^{-1} \left(\Phi_{rv}^T \Phi_{rr} + q \Phi_{vv}^T \Phi_{vr}\right) \delta \mathbf{r}_j - \delta \mathbf{v}_j \tag{8}$$

where $\Phi_{rr}, \Phi_{rv}, \Phi_{vr}$, and Φ_{vv} are the 3-by-3 blocks of $\Phi\left(t_j, t_{j+1}\right)$, which is the State Transition Matrix (STM) associated to the nominal trajectory between two consecutive TCM times t_j and t_{j+1}, while $\delta \mathbf{r}$ and $\delta \mathbf{v}$ are the deviations with respect to the nominal trajectory. These are computed starting from the state estimate resulting from the OD process.

$$\begin{cases} \delta \mathbf{r} = \hat{\mathbf{r}} - \mathbf{r}^* \\ \delta \mathbf{v} = \hat{\mathbf{v}} - \mathbf{v}^* \end{cases} \tag{9}$$

The parameter q is used either to adjust dimensions or to change the guidance algorithm behavior, favoring position deviation at the expense of velocity deviation and vice versa. In this work, $q = 0.01$ has been selected according to the results presented in Reference 1.

NUMERICAL RESULTS

This section presents the numerical results obtained by applying the previously described method for robust mission design, starting with an introduction to the procedure used to achieve these results.

For the space-based navigation strategy, which relies on spacecraft-to-spacecraft measurements, the first step is selecting a beacon satellite to serve as the target for optical observations. In this case, a satellite in a NRHO is chosen, reflecting the high scientific interest in this orbital regime, particularly within the context of the ARTEMIS program. A key factor influencing navigation filter performance is the relative phase between the observer, LUMIO in this case, and the target. Therefore, a preliminary analysis to identify the optimal relative configuration is conducted as the initial step.

The next stage involves designing the nominal trajectory within a deterministic framework to generate an initial guess for the Multi-step approach. Multiple solutions can be found from this first optimization process, resulting in a dataset of nominal trajectories. This dataset is then used to select a reduced number of initial guesses, ensuring sufficient diversity in terms of different metrics. This selection allows for a comprehensive assessment of the robust optimization algorithm's performance acting on different solutions.

Finally, the results corresponding to these different initial guesses are presented, providing insights into the critical aspects of the optimization method and its effectiveness.

Beacon Orbit Selection

Given the high scientific interest, the NRHO has been selected as the orbital regime for the beacon satellite. For an actual implementation of the navigation scenario, an initial position on this orbit must be identified. This choice has been made through a preliminary numerical analysis relying on the use of the DAGDOP metric, which captures both the dynamic characteristics and the observation geometry of the navigation scenario.[16]

The DAGDOP is therefore used to identify the best initial phase with the LUMIO satellite placed at the beginning of its transfer leg and the beacon satellite. LUMIO is considered to be fixed at its initial position, while the choice for the initial position of the beacon satellite will be made according to the results of this preliminary analysis. In this way, by exploiting this choice for initial relative configuration, the navigation performance resulting from the use of the spacecraft-to-spacecraft method should be maximized.

For this specific case, as visible in Figure 6, the best relative placement is given when the beacon spacecraft is approximately at half of its orbit starting from the aposelenium. This consists in the LUMIO satellite placed at the beginning of its transfer leg and the beacon satellite at its periselenium. It is also possible to notice that appreciable performance should be reached with the beacon satellite in proximity of the aposelenium, thus always along the periapsis. This result can be justified by the fact that these relative configurations both allow for a sufficiently fast variation of the acquired measurements, which should imply a better convergence for the filter and a more accurate solution.

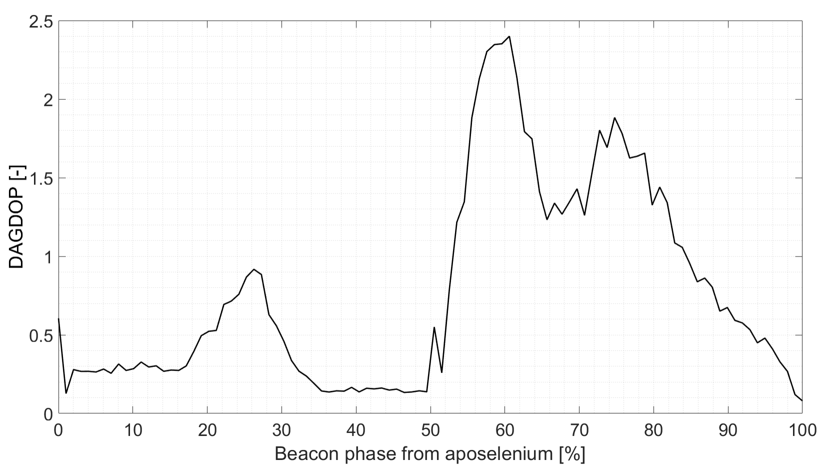

Figure 6. DAGDOP associated to orbit determination performance through optical-only measurements for the LUMIO orbital transfer leg as a function of the initial position of the beacon spacecraft on its orbit.

This preliminary analysis highlights a notable advantage of space-based navigation, which is its flexibility, offering more degrees of freedom during the mission design phase. The possibility to select the initial time of a mission phase based on the optimal configuration relative to the observation target is particularly beneficial, especially when compared to the restrictive viewing conditions imposed by the use of a specific ground stations for the acquisition of measurements.

Initial Guess

The procedure to be followed to get a nominal solution for the orbital transfer between the injection lunar orbit and the target halo orbit consists of several steps. First, a set of stable manifolds arriving onto the operative halo orbit is computed within a selected time span starting from 1 February 2024 to 1 March 2024, which can be considered as an interval for the potential arrival date. Then, given that some of the orbital parameters of the injection orbit are considered among the degrees of freedom, a set of lunar orbits is computed. The points of smaller distance between the back-propagated set of stable manifolds and the set of injection orbits are computed in order to filter out the ones exceeding a threshold of 250 km. Once a certain number of candidate solutions are found, they are given as initial guess to an optimization routine based on a single shooting framework that allows to guarantee the physical constraint of continuity in position between the manifold and the injection orbit while minimizing the fuel consumption given by the two deterministic impulses (SMIM and HIM). An example of a nominal solution for the transfer phase is given in Figure 7.

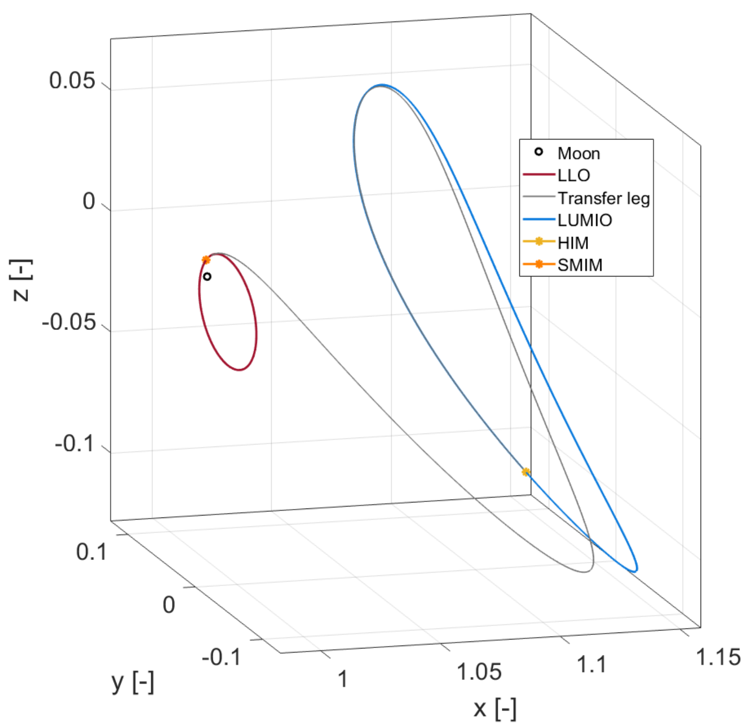

Figure 7. Example of LUMIO transfer from a low lunar orbit (LLO), represented in red, to the operative halo orbit, represented in blue. The SMIM and HIM maneuvers are reported respectively with an orange and a yellow dot.

Dataset Generation

For an exhaustive investigation of the selected navigation strategy, a dataset of nominal solutions for the transfer phase is firstly computed by exploiting the multiple candidates obtained from the operations explained in the previous section. For each of these solutions, the navigation assessment is performed according to the timeline of Figure 1, such that the metrics related to their stochastic costs, which are the 99-percentile of the two TCMs (denoted as Q1 and Q2) and the CDF of the final dispersion (denoted as Fd), are computed. This is done in order to get a first quantification of the overall performance of the different solutions in terms of robustness in order to make a selection and get a representative dataset that may help in drawing relevant considerations. To ensure a fair comparison, these metrics are calculated using both the ground-based and the space-based navigation strategies for providing the state estimate that is then used for the computation of the TCMs. The ground-based navigation method will be referred to as GB, while the space-based one as SB.

To compute these stochastic metrics, the navigation assessment requires the definition of an initial covariance to represent the uncertainty in the spacecraft's state. Following the motivations and the numerical values given in Reference 1, the initial covariance is assigned after the execution of the first impulsive maneuver. This approach simultaneously accounts for initial navigation errors and maneuver execution errors, thereby reducing the number of random variables to consider.

Both the deterministic and stochastic metrics are evaluated and reported in Figure 8 and in Figure 9. For the deterministic ones, the red dots correspond to the first impulsive maneuver, while the blue dots to the second. For the stochastic ones, the blue dots correspond to ground-based navigation and the red dots to the space-based navigation. From the plots, one can immediately note that some solutions are very similar, but also that it is possible to make a choice in order to guarantee a sufficient variety.

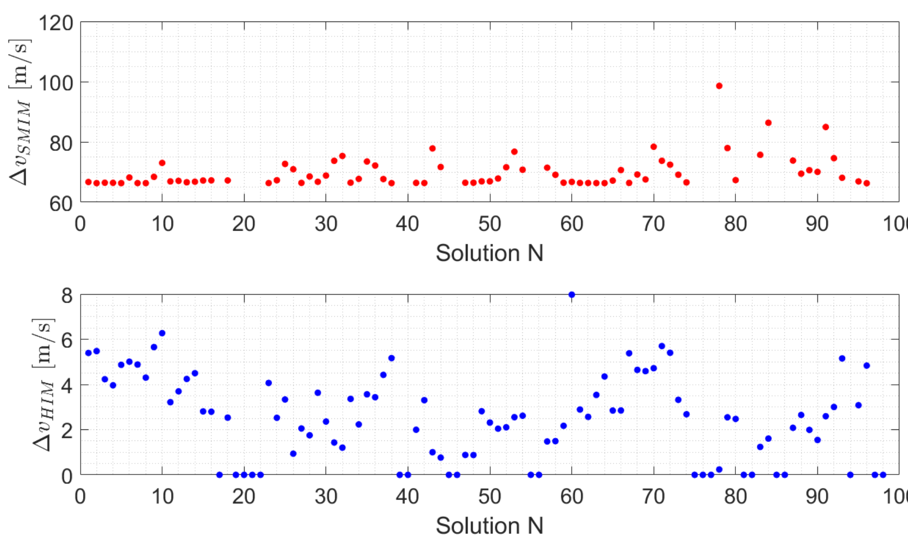

Figure 8. Values of the deterministic costs associated to the complete dataset of nominal solutions. First row is for the SMIM, while the second row is for the HIM.

According to the goal of ensuring this variety, four nominal solutions have been selected and

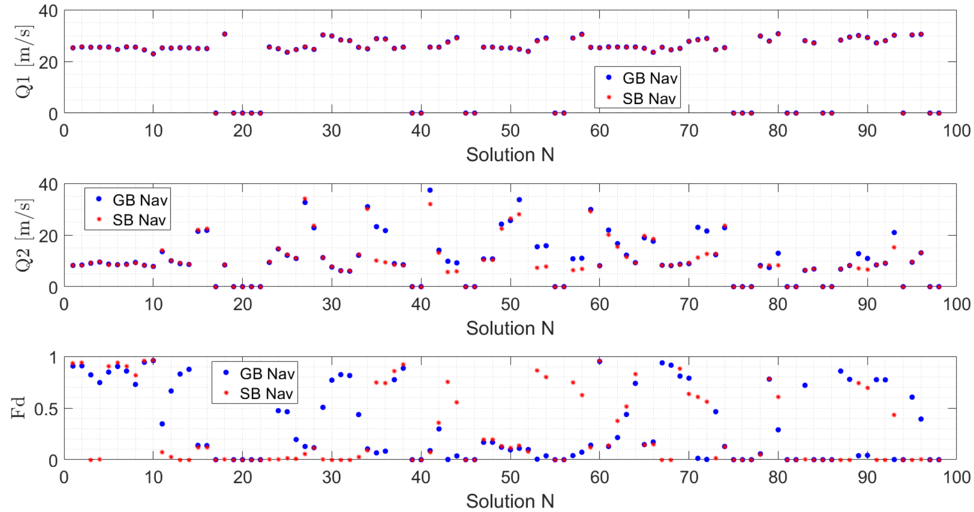

Figure 9. Metrics associated to the complete dataset of nominal solutions. First row is for the 99-percentile of the first TCM, second row is for the 99-percentile of the second TCM, third row is for the CDF of the final dispersion. Blue dots correspond to ground-based navigation. Red dots correspond to space-based navigation.

reported in Table 3. Solution *14* has been selected for the value of the final dispersion, which is higher for the GB than for the SB. Solution *50* presents low values in the final dispersion for both the navigation methods. Solution *90* shows a difference between the costs of the second TCM, and a large difference in the final dispersion between the two navigation methods, which highlights, since the typical sequential approach phase, the possible advantage given by the use of a space-based strategy. Finally, solution *11* has been selected because of the failure of the optimization process based on the SB strategy, which allows to investigate the sensitivity to some relevant parameters.

Table 3. Deterministic impulses and stochastic metrics related to the final dataset of nominal solutions for the transfer phase.

ID	$\Delta v_{\mathbf{HIM}}$ [m/s]	$\Delta v_{\mathbf{SMIM}}$ [m/s]	**Q1** [m/s]		**Q2** [m/s]		**Fd**	
-	-	-	**GB**	**SB**	**GB**	**SB**	**GB**	**SB**
11	3.09	66.81	25.22	25.21	15.32	15.81	0.253	0.103
14	4.16	66.77	25.23	25.21	9.02	9.17	0.809	0.000
50	2.31	66.91	25.24	25.27	25.61	25.30	0.095	0.113
90	1.52	70.38	29.80	29.66	11.03	6.61	0.047	0.674

Optimization Results

The results obtained from the optimization method begin with an analysis of the variations in fuel consumption for the four previously selected solutions. Specifically, Table 4 displays the fuel consumption values obtained using the SA, while Table 5 presents the values after applying the Multi-step approach. The main point to note is the reduction in stochastic costs for all solutions, except for solution 11 in the case of the SB strategy. This result will be further analyzed at the end of this section, emphasizing key factors affecting the robustness of the solution.

Table 4. Final dataset of nominal solutions: fuel consumption resulting from the application of the sequential approach according to the default mission timeline.

ID	**Tot Det** [m/s]	**Tot Stoc** [m/s]		**Tot** [m/s]	
-	-	**GB**	**SB**	**GB**	**SB**
11	69.90	40.54	41.03	110.44	110.93
14	70.92	34.24	34.38	105.17	105.30
50	69.22	50.85	51.57	120.07	120.79
90	71.90	40.83	36.27	112.73	108.17

Table 5. Final dataset of nominal solutions: optimized fuel consumption resulting from the application of the Multi-step approach divided in total deterministic, stochastic, and overall costs.

ID	**Tot Det** [m/s]	**Tot Stoc** [m/s]		**Tot** [m/s]	
-	-	**GB**	**SB**	**GB**	**SB**
11	69.90	22.96	90.97	92.87	160.87
14	70.92	21.20	21.13	92.12	92.05
50	69.22	22.54	22.03	91.76	91.25
90	71.90	37.15	22.91	109.06	94.82

In order to better investigate the effects of the optimization procedure, solution 50 is selected to show more detailed results. In particular, the results in terms of stochastic costs and final dispersion are show in Table 6 for all the steps of the robust mission design approach, starting from the values obtained from the application of the standard sequential approach. In this way it is possible to appreciate which are the steps of the optimization algorithm that have the largest impact on the metrics of interest. In general, the last three columns of Table 6 show that the goal is achieved with both the navigation methods, since the 99-percentile of the two TCMs is reduced and the value of the CDF related to the final dispersion is increased.

Analyzing the table more in detail, the results from the P-IA step show a significant reduction in the stochastic cost associated with the TCMs, even though the final dispersion does not yet meet the imposed constraint. This is visibly improved in the subsequent steps of the optimization procedure. These findings emphasize the crucial role of selecting the optimal epoch for executing TCMs, underlining their importance in enhancing the robustness of the solution.

The N-IA step further improves robustness by reducing both the stochastic costs and the final dispersion through an optimal selection of the navigation windows. This enables better state estimation performance, resulting in more accurate TCM calculations and a lower final dispersion.

Interestingly, the application of the F-IA step does not yield noticeable improvements compared to the previous steps, indicating that the initial guess provided to the optimization algorithm is

Table 6. Results of the application of the optimization sequence on solution *50*. The first four rows are for the ground-based strategy. The last four rows are for the space-based strategy.

Nav	**Algo**	$\Delta v_{\mathbf{HIM}}$ [m/s]	$\Delta v_{\mathbf{SMIM}}$ [m/s]	**Q1** [m/s]	**Q2** [m/s]	**Fd**
GB	SA	2.31	66.91	25.24	25.61	0.095
GB	P-IA	2.31	66.91	18.47	8.28	0.774
GB	N-IA	2.31	66.91	17.08	5.47	0.929
GB	F-IA	2.30	66.90	17.07	5.47	0.930
SB	SA	2.31	66.91	25.27	26.30	0.113
SB	P-IA	2.31	66.91	17.29	5.03	0.925
SB	N-IA	2.31	66.91	17.14	4.91	0.944
SB	F-IA	2.31	66.91	17.14	4.89	0.946

already close to an optimal solution. This result also suggests that certain optimization variables have a more significant impact on the robustness of the solution than others.

Following the previous considerations, given the nature of the P-IA and the N-IA algorithms, where the free variables are related only to the navigation assessment part, an important outcome is that, while the deterministic costs clearly remain the same, the stochastic costs are relevantly reduced leading also to the compliance with the desired final constraint. Following this, the results obtained from the F-IA, which is applied as a final step, indicate that the variables exhibiting the highest sensitivity for ensuring the success of the optimization process are the TCM epochs and the OD windows. This highlights which are the key variables playing the most valuable role in increasing the robustness of the initial solution. The main goal of the F-IA was to find optimal solutions that are very close to the initial guess (which is already a feasible solution for the transfer phase). Therefore, its job is not to find a completely new nominal solution, but to find a neighborhood solution which is feasible according to the new stochastic constraints. One of the main outcomes is that we are able to optimize the stochastic costs of a nominal solution by acting directly on the variables strictly connected to the navigation assessment, without necessarily modifying the initial solution. On the other hand, one of the most interesting aspects of the F-IA is that it is able to reduce the deterministic costs as well, which is anyway accomplished even if with very small changes.

For solution 11, which does not produce interesting results, a deeper analysis on the reasons of the failure has been conducted. In fact, a simple reason for the failure of the optimization process may be that the navigation windows are too small, or that the relative geometry conditions do not allow effective measurement acquisition. This would cause a lack of convergence during the state estimation algorithm and, therefore, poor stochastic performance. This may be solved by modifying the conditions for the navigation operations. For the GB strategy, this implies selecting a different ground station or shifting the mission timeline. For the SB one, it may imply selecting another beacon satellite or starting with a different relative phase.[16] Another relevant factor for both strategies could be the frequency of measurement acquisition. It must be emphasized that by adjusting these key factors, both navigation strategies could be rendered effective. For these reasons, it was actually proven that a valuable choice for each of the just mentioned parameters can lead to greater performance of the selected solution. To evaluate the performance of the SB strategy for solution 11, certain conditions are modified. Table 7 presents the results of the optimization process with only one condition changed at a time compared to the previous setup. First, the measurement acquisition frequency is adjusted from 10 minutes to 5 minutes. Next, the relative phase between LUMIO and the beacon spacecraft is altered. Lastly, the beacon spacecraft is placed in a different orbit, specifically a Distant Retrograde Orbit (DRO).

Table 7. Sensitivity analysis on the results of solution 11: optimized fuel consumption and final dispersion

ID	**Tot Det** [m/s]	**Tot Stoc** [m/s]	**Tot** [m/s]	**Fd**
11 SA	69.90	41.03	110.93	0.103
11 MS-IA	69.90	90.97	160.87	0.089
11 Freq	69.90	21.59	91.49	0.962
11 Phase	69.90	21.45	91.35	0.950
11 Orbit	69.90	21.63	91.53	0.974

The results in Table 7 clearly show that the initial application of the Multi-step approach (MS-IA) yields worse performance compared to the SA, as also observed in the previous tables. The third row illustrates the impact of increasing the measurement acquisition frequency, the fourth row reflects the effects of changing the relative phase with the beacon spacecraft, and the fifth row demonstrates the outcome of changing the beacon's orbit to a DRO.

All modifications to the original setup successfully improve the results coming from the optimization procedure, reducing both the stochastic costs and the final dispersion. This result underscores the importance of accurately selecting elements that affect the navigation performance and, consequently, the robustness of the solution. Furthermore, it highlights the flexibility provided by a space-based navigation strategy, which increases the degrees of freedom during the mission design phase and expands the range of feasible solutions.

CONCLUSION

The goal of this work was to evaluate the potential of a fully autonomous spacecraft-to-spacecraft optical-only navigation strategy within a robust mission design framework. The analysis and results presented highlight several factors influencing the performance of this methodology. Notably, the differences between ground-based and space-based navigation strategies were emphasized, with the latter offering shorter observer-to-target distances, enabling more efficient target observations. However, challenges generated by the rapidly changing relative geometries, such as exclusion angles, occulting bodies, and eclipses were also identified. Additionally, the need for appropriate onboard hardware to acquire optical measurements was underlined, given the limitations observed in both ground-based and early space-based operations.

A key finding of this work is that the space-based navigation strategy demonstrated performance comparable to traditional ground-based methods. Another critical advantage is the flexibility offered by space-based navigation, with additional degrees of freedom such as adjusting the relative phase between the observer and target or selecting the beacon orbit. This flexibility becomes increasingly valuable as the number of spacecraft in cislunar space grows.

The benefits of using a revised mission design approach that incorporates uncertainties directly into the optimization process were also highlighted. This method avoids the limitations of standard sequential approaches, which often rely on trial-and-error procedures, by providing a more systematic path to optimal solutions. A crucial element of this approach is the uncertainty quantification method based on PCE-CUT, which enables the efficient generation of Monte Carlo-like samples and facilitates the computation of stochastic costs during the optimization process.

This study has demonstrated the advantages of an autonomous navigation strategy in addressing the growing workload on ground stations and evaluated the potential of spacecraft-to-spacecraft optical-only measurements as a viable alternative for the computation of robust solutions in cislunar space. These findings are particularly relevant in the context of the increasing number of lunar missions relying on the use small spacecraft with limited capabilities.

REFERENCES

[1] C. Giordano and F. Topputo, "Analysis, Design, and Optimization of Robust Trajectories in Cislunar Environment for Limited-Capability Spacecraft," *The Journal of the Astronautical Sciences*, Vol. 70, No. 6, 2023, p. 53.

[2] M. J. Holzinger, C. C. Chow, and P. Garretson, "A primer on cislunar space," 2021.

[3] P. Panicucci, F. Piccolo, A. Rizza, G. Merisio, F. Topputo, R. Walker, *et al.*, "Vision-Based Navigation for the LUMIO CubeSat Mission," *46th AAS Guidance, Navigation and Control Conference*, 2024, pp. 1–20.

[4] K. Hill and G. H. Born, "Autonomous interplanetary orbit determination using satellite-to-satellite tracking," *Journal of guidance, control, and dynamics*, Vol. 30, No. 3, 2007, pp. 679–686.

[5] J. A. Greaves and D. J. Scheeres, "Autonomous Optical-Only Spacecraft-to-Spacecraft Absolute Tracking and Maneuver Classification in Cislunar Space," *Journal of Guidance, Control, and Dynamics*, Vol. 46, No. 11, 2023, pp. 2092–2109.

[6] A. Cervone, F. Topputo, S. Speretta, A. Menicucci, E. Turan, P. Di Lizia, M. Massari, V. Franzese, C. Giordano, G. Merisio, *et al.*, "LUMIO: A CubeSat for observing and characterizing micro-meteoroid impacts on the lunar far side," *Acta Astronautica*, Vol. 195, 2022, pp. 309–317.

[7] V. Szebehely and E. Grebenikov, "Theory of Orbits-The Restricted Problem of Three Bodies.," *Soviet Astronomy, Vol. 13, p. 364*, Vol. 13, 1969, p. 364.

[8] A. M. Cipriano, D. A. Dei Tos, and F. Topputo, "Orbit design for LUMIO: The lunar meteoroid impacts observer," *Frontiers in Astronomy and Space Sciences*, Vol. 5, 2018, p. 29.

[9] N. Adurthi and P. Singla, "Conjugate unscented transformation-based approach for accurate conjunction analysis," *Journal of Guidance, Control, and Dynamics*, Vol. 38, No. 9, 2015, pp. 1642–1658.

[10] M. Hejduk, "Specular and diffuse components in spherical satellite photometric modeling," *Proceedings of the Advanced Maui Optical and Space Surveillance Technologies Conference*, 2011, pp. 1–11.

[11] C. Frueh, B. Little, and J. McGraw, "Optical sensor model and its effects on the design of sensor networks and tracking," *Advanced Maui Optical and Space Surveillance Technologies Conference (AMOS)*, 2019.

[12] T. A. Pavlak, *Trajectory design and orbit maintenance strategies in multi-body dynamical regimes*. PhD thesis, Purdue University, 2013.

[13] V. K. Srivastava, M. Pitchaimani, B. Chandrasekhar, *et al.*, "Eclipse prediction methods for LEO satellites with cylindrical and cone geometries: a comparative study of ECSM and ESCM to IRS satellites," *Astronomy and Computing*, Vol. 2, 2013, pp. 11–17.

[14] F. Markley and J. Crassidis, *Fundamentals of Spacecraft Attitude Determination and Control*. Space Technology Library, Springer New York, 2014.

[15] D. A. Dei Tos, M. Rasotto, F. Renk, and F. Topputo, "LISA Pathfinder mission extension: A feasibility analysis," *Advances in Space Research*, Vol. 63, No. 12, 2019, pp. 3863–3883.

[16] Z.-Y. Gao and X.-Y. Hou, "Comparison of Autonomous Orbit Determination for Satellite Pairs in Lunar Halo and Distant Retrograde Orbits," *NAVIGATION: Journal of the Institute of Navigation*, Vol. 69, No. 2, 2022.